PHYSICAL REVIEW D **84,** 034014 (2011)

Pion-photon transition: The new QCD frontier

A. P. Bakulev,[1,*] S. V. Mikhailov,[1,†] A. V. Pimikov,[1,‡] and N. G. Stefanis[2,§]

[1]*Bogoliubov Laboratory of Theoretical Physics, JINR, 141980 Dubna, Russia*

[2]*Institut für Theoretische Physik II, Ruhr-Universität Bochum, D-44780 Bochum, Germany*

(Received 2 June 2011; published 8 August 2011)

We perform a detailed analysis of all existing data (CELLO, CLEO, *BABAR*) on the pion-photon transition form factor by means of light-cone sum rules in which we include the next-to-leading order QCD radiative corrections and the twist-four contributions. The next-to-next-to-leading order radiative correction together with the twist-six contribution are also taken into account in terms of theoretical uncertainties. Keeping only the first two Gegenbauer coefficients a_2 and a_4, we show that the 1σ error ellipse of all data up to 9 GeV^2 greatly overlaps with the set of pion distribution amplitudes obtained from nonlocal QCD sum rules—within the range of uncertainties due to twist-four. This remains valid also for the projection of the 1σ error ellipsoid on the (a_2, a_4) plane when including a_6. We argue that it is not possible to accommodate the high-Q^2 tail of the *BABAR* data with the same accuracy, despite opposite claims by other authors, and conclude that the *BABAR* data still pose a challenge to QCD.

DOI: 10.1103/PhysRevD.84.034014 PACS numbers: 12.38.Lg, 11.10.Hi, 12.38.Bx, 13.40.Gp

I. INTRODUCTION

The pion-photon transition $\gamma^* + \gamma^* \to \pi^0$ is an example par excellence of an exclusive process that can be adequately described within QCD by virtue of collinear factorization, provided both photon virtualities are sufficiently large (for a review, see [1]). Then, the transition form factor, defined by the correlator of two electromagnetic currents

$$\int d^4z e^{-iq_1\cdot z}\langle \pi^0(P) \mid T\{j_\mu(z)j_\nu(0)\} \mid 0\rangle = i\epsilon_{\mu\nu\alpha\beta}q_1^\alpha q_2^\beta F^{\gamma^*\gamma^*\pi}(Q^2, q^2) \tag{1}$$

with $Q^2 \equiv -q_1^2 > 0$, $q^2 \equiv -q_2^2 \geq 0$, can be recast in leading-twist approximation in the convolution form [2,3]

$$F^{\gamma^*\gamma^*\pi}(Q^2, q^2) = \frac{\sqrt{2}}{3} f_\pi \int_0^1 dx T(Q^2, q^2, \mu_F^2, x) \times \varphi_\pi^{(2)}(x, \mu_F^2) + O(\delta^2/Q^4), \tag{2}$$

where the pion decay constant is $f_\pi = 132$ MeV, δ^2 is the twist-four coupling, and where we assumed that the photon momenta are sufficiently large $Q^2, q^2 \gg m_\rho^2$. This way, the quark-gluon subprocesses, encoded in the hard-scattering amplitude T, can be systematically computed order-by-order within QCD perturbation theory. The binding (nonperturbative) effects are separated out and absorbed into a universal pion distribution amplitude (DA) of twist-two $\varphi_\pi^{(2)}(x, \mu^2)$, defined first in [4]. The variation of $\varphi_\pi^{(2)}(x, \mu^2)$ with the factorization scale μ^2 is controlled by the Efremov-Radyushkin-Brodsky-Lepage (ERBL) renormalization group evolution equation [2,3]. This implies that the pion DA can be expressed in terms of the Gegenbauer polynomials $C_n^{3/2}(2x-1)$ to read

$$\varphi^{(2)}(x, \mu^2) = \varphi^{\rm as}(x) + \sum_{n=2,4,\ldots} a_n(\mu^2)\psi_n(x), \tag{3}$$

where $\psi_n(x) = 6x(1-x)C_n^{3/2}(2x-1)$ and $\varphi^{\rm as}(x) = \psi_0(x) = 6x(1-x)$ is the asymptotic pion DA [2,3].

The coefficients a_n $(n \geqq 2)$ have to be determined within some nonperturbative model or be extracted from the data, taking into account evolution effects to account for their momentum-scale dependence. In most theoretical analyses they are derived from the moments $\langle \xi^N \rangle_\pi \equiv \int_0^1 dx(2x-1)^N \varphi_\pi^{(2)}(x, \mu^2)$ with the normalization condition $\int_0^1 dx \varphi_\pi^{(2)}(x, \mu^2) = 1$.

A process with two photons of high virtuality cannot be easily measured experimentally. Experimental information is mostly available for an asymmetric configuration in which one of the photons is quasi-on-mass-shell with $q^2 \to 0$ [5–7]. In that case, perturbative QCD cannot be directly applied at a consolidated level because the real photon is emitted at large distances and has, therefore, a hadronic content that demands the application of nonperturbative techniques. Such a method is provided by light-cone sum rules (LCSRs) [8] (a recent application of this method to the pion-photon transition form factor is given in [9]) that augment QCD perturbation theory in approaching the real photon via a dispersion relation for $F^{\gamma^*\gamma^*\pi}$ in the variable q^2, keeping the large variable Q^2 fixed, viz.,

$$F^{\gamma^*\gamma^*\pi}(Q^2, q^2) = \int_0^\infty ds \frac{\rho(Q^2, s)}{s + q^2}, \tag{4}$$

where the physical spectral density $\rho(Q^2, s)$ approaches at large s the perturbative one:

*bakulev@theor.jinr.ru
†mikhs@theor.jinr.ru
‡pimikov@theor.jinr.ru
§stefanis@tp2.ruhr-uni-bochum.de

$$\rho^{\rm PT}(Q^2, s) = \frac{1}{\pi}\,{\rm Im}F^{\gamma^*\gamma^*\pi}(Q^2, -s - i\varepsilon). \tag{5}$$

The resulting LCSR can be written as follows:

$$Q^2F^{\gamma^*\gamma\pi}(Q^2) = \frac{Q^2}{m_\rho^2}\int_{x_0}^1 \exp\left(\frac{m_\rho^2 - Q^2\bar{x}/x}{M^2}\right)\bar{\rho}(Q^2, x)\frac{dx}{x} + \int_0^{x_0}\bar{\rho}(Q^2, x)\frac{dx}{\bar{x}} \tag{6}$$

with the spectral density $\bar{\rho}(Q^2, x) = (Q^2 + s)\rho^{\rm PT}(Q^2, s)$ and the abbreviations $s = \bar{x}Q^2/x$ and $x_0 = Q^2/(Q^2 + s_0)$. The first term in (6) stems from the hadronic content of a quasireal photon at low $s \le s_0$, while the second one resembles its pointlike behavior at higher $s > s_0$. The hadronic threshold in the vector-meson channel has the value $s_0 = 1.5$ GeV^2, whereas $m_\rho = 0.77$ GeV [10]. The Borel parameter M^2 entering the LCSR in (6) is not varied aiming to obtain the best stability of the LCSR. It is actually specified via $M^2 = M^2_{2\text{-pt}}/\langle x\rangle_{Q^2}$ from the two-point QCD sum rule for the ρ-meson, where the corresponding Borel parameter is $M^2_{2\text{-pt}} \in [0.5 \div 0.8]$ GeV^2. Here, $\langle x\rangle_{Q^2}$ is some average value of x at a fixed scale Q^2 in the integration region for the first integral on the right-hand side of Eq. (6), i.e., $x_0(Q^2) < \langle x\rangle_{Q^2} < 1$—see also [8].

The remainder of the paper is organized as follows. In the next section, we review the current understanding of the experimental data on the pion-photon transition form factor, focusing on the problems related to the unexpected rise of the *BABAR* data [7] beyond 10 GeV^2. In Sec. III, we present the salient features of a calculation of the pion-photon transition form factor using LCSRs with next-to-leading order (NLO) accuracy and including the twist-four contribution. The results of our calculation are presented and discussed in detail in Sec. IV in terms of two tables and several figures, paying particular attention to the intrinsic theoretical uncertainties stemming from various sources. Finally, a summary of our main findings is given in Sec. V, where we also draw our conclusions.

II. STATUS OF EXPERIMENTAL DATA

Using the method of LCSRs with fixed $M^2 = 0.7$ GeV^2, Schmedding and Yakovlev (SY) [11] performed a NLO QCD analysis of the data on $F^{\gamma^*\gamma\pi}$, obtained by the CLEO Collaboration [6], with the inclusion of twist-four contributions, which they modeled by the asymptotic form, notably, [8,12]

$$\varphi_\pi^{(4)}(x, \mu^2) = (80/3)\delta^2(\mu^2)x^2(1 - x)^2. \tag{7}$$

The major outcome of their analysis was that the best agreement with these high-precision data can be achieved by a pion DA with the coefficients $a_2^{\rm SY}(\mu^2_{\rm SY} \equiv 5.76\ {\rm GeV}^2) = 0.19$, $a_4^{\rm SY}(\mu^2_{\rm SY}) = -0.14$, which after evolution to the reference scale $\mu_1^2 \equiv 1$ GeV^2 [13] become $a_2^{\rm SY}(\mu_1^2) = 0.27$, $a_4^{\rm SY}(\mu_1^2) = -0.22$.

At the same time, the asymptotic pion DA and the Chernyak-Zhitnitsky (CZ) model [14] with $a_2^{\rm CZ}(\mu_1^2) = 0.56$ and $a_4 = 0$ were found to be outside the 2σ level.[1] Later, this type of analysis was refined in [15,16] by taking into account the correct ERBL evolution of the pion DA to each measured momentum, including also the variation of the twist-four coupling $\delta^2 \equiv \delta^2(\mu_1^2) = 0.19 \pm 0.04$ GeV^2 in (7). This way it was shown that the DAs $\varphi_\pi^{\rm as}$ and $\varphi_\pi^{\rm CZ}$ are outside the 3σ and 4σ error ellipses, respectively, while the best fit yields $\chi^2_{\rm ndf} = 0.47$ (where ndf denotes the number of degrees of freedom); see [16] for more details.

Even more important is the fact that the 1σ error ellipse[2] of the CLEO data strongly overlaps with the admissible values of the coefficients a_2 and a_4, determined before in the framework of QCD sum rules with nonlocal condensates (NLC SRs) [17]. In particular, we proposed a "bunch" of admissible pion DAs with the central point $a_2^{\rm BMS}(\mu_1^2) = 0.20$ and $a_4^{\rm BMS}(\mu_1^2) = -0.14$ (termed the BMS model) that turns out to be within the 1σ error ellipse of the CLEO data [6]. These pion DAs (and similar ones obtained by two of us (BP) in [18,19] by employing an extended version of the Gaussian model of the nonlocal QCD vacuum) have a distinctive feature: their endpoints at $x = 0$ and $x = 1$ are strongly suppressed—even relative to the asymptotic pion DA. This suppression is due to the finite virtuality $\lambda_q^2 = \langle\bar{q}(ig\sigma_{\mu\nu}G^{\mu\nu})q\rangle/(2\langle\bar{q}q\rangle) = (0.4 - 0.5)$ GeV^2 of the vacuum quarks, which enters the NLC SR for $\varphi_\pi^{(2)}$ in terms of the various condensate contributions (more details can be found in [17,20]).

These findings remain valid even if one assumes a much stronger contribution from the twist-four pion DA, as estimated in [13] using the renormalon model [21] (see also [22]). The calculation of $F^{\gamma^*\gamma\pi}$ beyond the NLO was carried out in [23] by taking into account that part of the next-to-next-to-leading order (NNLO) correction that is proportional to the first coefficient β_0 of the β function, known from the earlier work in [24]. It turns out that this radiative correction is negative, thus providing *suppression* of the form factor at the level of about 8%, slowly decreasing with increasing Q^2. To the extent that one's ambition is to comply with the CLEO data on $\gamma^*\gamma \to \pi^0$, it is mandatory to have a pion DA that has its endpoints $x = 0, 1$ suppressed with a moderate dip at $x = 1/2$, just as the BMS model extracted from NLC SRs. It is worth mentioning that this model gives rise to a scaled form factor $Q^2F^{\gamma^*\gamma\pi}(Q^2)$ that approaches the asymptotic limit $\sqrt{2}f_\pi$,

[1] The value of $a_2^{\rm CZ}$ was originally determined by Chernyak and Zhitnitsky at the (low) scale $\mu^2_{\rm CZ} = 0.25$ GeV^2 [14] and reads $a_2^{\rm CZ}(\mu^2_{\rm CZ}) = 2/3$. Its determination at the usual reference scale $\mu_1^2 = 1$ GeV^2 is described in Appendix B of Ref. [15].

[2] Here and below we denote by 1σ ellipse (ellipsoid) a confidence region in the (a_2, a_4) plane that represents a coverage probability equal to 68.27%.

predicted by perturbative QCD, from *below*, while at low momenta it also yields reasonable agreement with the CELLO data [5].[3] Therefore, it came as a surprise that the data on $\gamma\gamma^* \to \pi^0$, presented by the *BABAR* Collaboration in 2009 [7], indicate above approximately 10 GeV^2 a marked growth of the form factor with Q^2 (see upper points (labeled by open crosses) in Fig. 1 taken from [25]). In fact, the *BABAR* Collaboration fitted their data with the expression

$$Q^2 F^{\gamma^*\gamma\pi} \sim \left(\frac{Q^2}{10\ \text{GeV}^2}\right)^{\beta}, \tag{8}$$

where $\beta = 0.25 \pm 0.02$, i.e., $F^{\gamma^*\gamma\pi} \sim Q^{-3/2}$. This behavior of the form factor is incompatible with the collinear factorization and exceeds the asymptotic prediction considerably up to the highest measured momentum value just below 40 GeV^2. Moreover, the high-Q^2 *BABAR* tail contradicts the CLEO data that are well described by the dipole fit [6]

$$Q^2 F^{\gamma^*\gamma\pi} \sim \frac{Q^2}{Q^2 + \Lambda^2} \tag{9}$$

with $\Lambda \approx 776$ MeV. This scale behavior becomes more puzzling by comparing the π^0 *BABAR* data with the predictions extracted by the *BABAR* Collaboration from their analysis of the two-photon η and η' decays [25]—Fig. 1. While the direct π^0 data grow with Q^2 and necessitate a wide DA with strong contributions from the endpoint regions $x = 0$, 1, the converted η-η' data are in perfect agreement with the prediction obtained with the endpoint-suppressed BMS pion DA (solid line in Fig. 1). To describe both sets of the *BABAR* data with the *same* accuracy looks like a catch-22 situation because it demands an impossible compromise for the structure of the pion DA (more on this and its implications later).

Many theorists have attempted during the past two years to explain the rise of the *BABAR* data using various schemes and drawing incongruent conclusions. We may group these theoretical proposals into four categories:

(i) Abandon collinear factorization: An increase of the form factor with Q^2 can be achieved by employing a flat-top pion DA, as proposed by Radyushkin [26] and by Polyakov [27]—which used, however, different schemes. The key element of these approaches is a nonvanishing pion DA at the endpoints $x = 0$, 1. Such a pion DA ascribes the rise of the large-Q^2 tail of the *BABAR* data to a logarithmic increase of the form factor induced by the flat-top DA. Note, incidentally, that as shown in [28], a $\ln Q^2$ behavior can actually be imitated by including just the first three Gegenbauer polynomials without demanding the flatness of the pion DA. However, one has to pay a high price for this agreement: already the NLO contribution at the default normalization scale $\mu^2 = Q^2$ turns out to be huge for the flat-top DA, forcing a much lower normalization scale below Λ_{QCD} and making it virtually impossible to include evolution effects which are at the heart of QCD.

(ii) Deny rise of the form factor: Very recently, Agaev *et al.* [9] argued that the trend of the high-Q^2 tail of the π^0 *BABAR* data can be reproduced within QCD using LCSRs. Their analysis of the form factor includes radiative corrections at the NLO level, twist-four contributions, and, for the first time, also a twist-six term which, though it has a positive sign, turns out to be small for their choice of the Borel parameter $M^2 = 1.5$ GeV^2 to provide any serious enhancement.[4] The distinctive feature of their models for the pion DA is a large and positive coefficient a_4 to which they attribute the rise of the form factor at high Q^2, while still higher coefficients a_n up to $n = 12$ have smaller values. The best agreement with the π^0 *BABAR* data [7] is provided by a modified flatlike DA with $a_2 = 0.13$, which has a large tail of Gegenbauer coefficients, while the other two considered models are given by truncated expansions with a_n up to $n = 8$ and provide form-factor predictions that almost scale with Q^2, but having a normalization exceeding considerably the asymptotic limit of $\sqrt{2} f_\pi$. Even the model with a_n

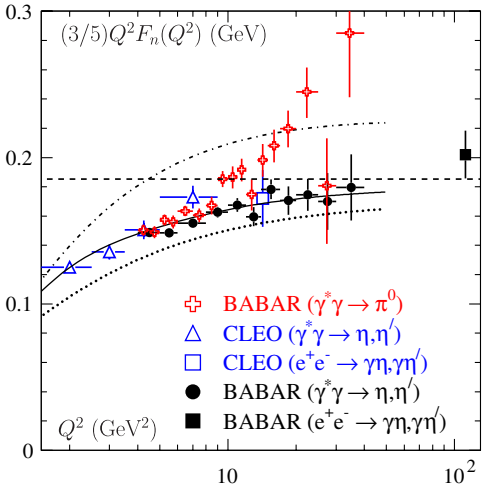

FIG. 1 (color online). The $\gamma\gamma^* \to |n\rangle$ transition form factor multiplied by 3/5 in comparison with $Q^2 F^{\gamma\gamma^*\pi}(Q^2)$ [7]. The dashed line indicates the asymptotic limit for $Q^2 F^{\gamma\gamma^*\pi}(Q^2)$. The dotted, dashed-dotted, and solid curves show the predictions from [15,16] for the asymptotic, the CZ, and the BMS DA, respectively (figure taken from [25]).

[3]Note that at low momenta close to $Q^2 \approx 1$ GeV^2, the twist-two contribution becomes comparable in size with the twist-four term.

[4]This fact is emphasized by these authors as being rather crucial in selecting that large value of the Borel parameter.

coefficients up to $n = 12$, which become successively operative with increasing Q^2, cannot simulate the increase of the form factor sufficiently well in comparison with the *BABAR* fit (8) used in [7]—provided one takes this fit seriously. At the same time, as one may appreciate from Fig. 1, all these models overestimate the *BABAR* data [25] on the $\gamma\gamma^* \to \eta(\eta')$ transition form factor significantly. Taking into account the NNLO radiative corrections would somewhat reduce the magnitude of the form factor by a few percent [23], but incorporating this effect would also shift the prediction further away from the $\gamma^*\gamma \to \pi^0$ *BABAR* data—the main goal. Thus, the conclusion drawn in [9] that one may achieve simultaneous agreement with all data on $F^{\gamma^*\gamma\pi}$ using LCSRs within QCD seems rather perfunctory. At the same time, the fact that the twist-six term turns out to have a positive sign renders Chernyak's recent claim in [29] that one can describe all data using the CZ DA supplemented by a power correction $1/Q^6$ with a huge negative coefficient $-(1.2\ \mathrm{GeV}^2)^2$ rather speculative.[5]

(iii) Contextual explanations: Various authors (e.g., [30]) have presented calculations of $Q^2F^{\gamma^*\gamma\pi}$ within the context of particular models—appealing, for instance, to the triangle anomaly—and have indeed obtained a logarithmic increase, emulating this way the large-Q^2 tail of the *BABAR* data. The problem with such approaches is that they involve (nonperturbative) context-dependent mass scales that cannot be derived from QCD and are specific for this particular process.

(iv) $\boldsymbol{k}_\perp$ factorization: Some authors try to explain the increase of the form factor by retaining the partonic $\boldsymbol{k}_\perp$ degrees of freedom unintegrated and employing a modified $\boldsymbol{k}_\perp$ factorization approach; see for instance [31–34]. However, it is well known from previous research [35,36] that Sudakov effects and $\boldsymbol{k}_\perp$-generated power corrections give rather suppression than enhancement, albeit self-reinforcement is also possible [37]. This subject is, however, outside the scope of the present investigation; it will be discussed in detail elsewhere.

III. DATA ANALYSIS

The strategy of our investigation is to use LCSRs in order to process all available experimental data on the pion-photon transition form factor from different experiments [5–7], making some technical improvements relative to our previous works in [13,15,16,23], and extending the analysis to the level of three Gegenbauer coefficients a_2, a_4, a_6. The improvements and the applied algorithms are explained in detail below.

To compute the form factor, we employ the LCSR (6). In order to resolve the ρ and ω meson resonances, we employ not a simple δ-function ansatz but a finite-width Breit–Wigner form [8,23]. Adopting Khodjamirian's general arguments [8], we relate the Borel parameter M^2 in the LCSR (6) to the Borel parameter $M^2_{2\text{-pt}}$ entering the two-point QCD sum rule for the ρ meson [38]. Hence, instead of using the fixed value $M^2 = M_0^2 = 0.7\ \mathrm{GeV}^2$, as in our previous works [15,16,18,19,23], we write $M^2(Q^2) = M_0^2/\langle x\rangle_{Q^2}$, where the average $\langle x\rangle_{Q^2}$ is calculated by means of the Borel exponential $\exp[Q^2\bar{x}/(M_0^2 x)]$ in (6). This prescription amounts to $M^2(Q^2) \in [0.7 \div 0.9]\ \mathrm{GeV}^2$.

The key ingredients of our data-analysis procedure are the following:

(i) The NLO gluon radiative corrections in the spectral density are taken into account using a corrected expression with respect to Eq. (3.12) in [23] that does not contain the error pointed out in [9]. Note that this error does not affect the results of our previous calculations with LCSRs in [13,15,16,23]. We adopt the so-called default renormalization-scale setting and identify the factorization and the renormalization scale with the large photon virtuality Q^2. This avoids the appearance of (large) logarithms of these scales.

(ii) We take into account the twist-four contribution, allowing for a significant variation of the parameter $\delta^2 = 0.19\ \mathrm{GeV}^2$ in the range $0.15\ \mathrm{GeV}^2$ to $0.23\ \mathrm{GeV}^2$, referring the reader for a detailed discussion to our previous analysis in [16]. As already mentioned, the use of a nonasymptotic form for $\varphi_\pi^{(4)}$ would not affect the results significantly [13,22]. The parameter $\delta^2(\mu^2)$ is evolved with μ^2 according to the one-loop renormalization group equation, whereas other perturbative corrections to the twist-four contribution are ignored—expected to be small.

(iii) The evolution of the coefficients a_n is taken into account at the NLO level of accuracy using the QCD scale parameters $\Lambda^{(3)}_{\mathrm{QCD}} = 370\ \mathrm{MeV}$ and $\Lambda^{(4)}_{\mathrm{QCD}} = 304\ \mathrm{MeV}$, consistent with the NLO estimate $\alpha_s(M_Z^2) = 0.118$ [10].

(iv) The inclusion of the NNLO β_0 radiative correction to the form factor, calculated in [24] and used in the spectral density in [23], as well as the twist-six term, computed for the first time in [9], are taken into account implicitly within the theoretical uncertainties. Their explicit evaluation is relegated to a future dedicated investigation. This treatment of the two contributions in terms of uncertainties is justified by the fact that for the average value of $M^2(Q^2) \sim 0.75\ \mathrm{GeV}^2$ the net result appears to be

[5]However, other power corrections of different origin with negative sign cannot be excluded, but can hardly be accommodated within QCD.

small, decreasing with Q^2 from $+0.005$ at $Q^2 = 1$ GeV^2—where the twist-six term prevails—down to -0.003 at $Q^2 = 40$ GeV^2—where the NNLO correction becomes stronger. Note that in the calculation of the NNLO term only the convolution of the hard-scattering amplitude T_β with the asymptotic DA $\varphi^{\rm as}$ is taken into account (see [23] for more details). It is worth mentioning that this behavior is sensitive to the choice of the Borel scale adopted in our work. Would we use instead the value $M^2 = 1.5 \pm 0.5$ GeV^2, advocated for in [9], then the twist-six term would be much smaller and the net result would be everywhere negative and almost constant: ≈ -0.004.

IV. DISCUSSION OF RESULTS

To be able to make precise estimates of the influence of the high-Q^2 tail of the *BABAR* data on the form factors, we use two different data sets: one which collects all available data from three experiments [5–7] for the Q^2 region between 1 and 9 GeV^2 (termed for convenience "CLEO regime") and a second set which includes as well the high-Q^2 *BABAR* data up to about 40 GeV^2. These results are displayed in Fig. 2, left and right panel, respectively. In practice, this analysis procedure allows us to understand the role and relative strength of the coefficient a_6 in determining the characteristics of the 1σ error ellipsoid of each data set selection, shown in this figure by its principal axes and corresponding ellipses.

The middle point $(0.17, -0.14, 0.12)$ of the 1σ error ellipsoid in the left panel of Fig. 2, resulting from analyzing the data in the CLEO regime, corresponds to a rather good $\chi^2_{\rm ndf} \approx 0.4$. This ellipsoid is stretched along the axis a_6 and has a sizable intersection with the (a_2, a_4) plane, shown in the figure as a smaller ellipse inside the green rectangle. In contrast, the inclusion of the high-Q^2 *BABAR* data (right panel) forces the ellipsoid away from that plane to a new middle point $(0.18, -0.17, 0.31)$ with a worse value $\chi^2_{\rm ndf} \approx 1$. Observe that the projection of the ellipsoid on the (a_2, a_4) plane remains almost unchanged, while its middle point ▼ (red) moves slightly away from its previous location, albeit it still resides inside the region of the negative values of a_4. The fact of the matter is that both error ellipses mentioned above cover quite a large region of those values of the coefficients a_2 and a_4 that have been determined in [17] with the help of NLC SRs—slanted (green) rectangle in Fig. 2. In particular, the position of the BMS pion DA in the (a_2, a_4) plane is just inside both ellipses for the CLEO regime with respect to all data (left panel) and still inside the 2D projection when one takes into account also the *BABAR* data up to 40 GeV^2 (right panel).

To further quantify these considerations, we perform a more detailed data analysis with the focus on the (a_2, a_4) plane and show the results in Fig. 3. The left panel refers to the data selection for the Q^2 values in the CLEO regime, while the right panel shows the analogous findings for the second case when we implement the analysis by including

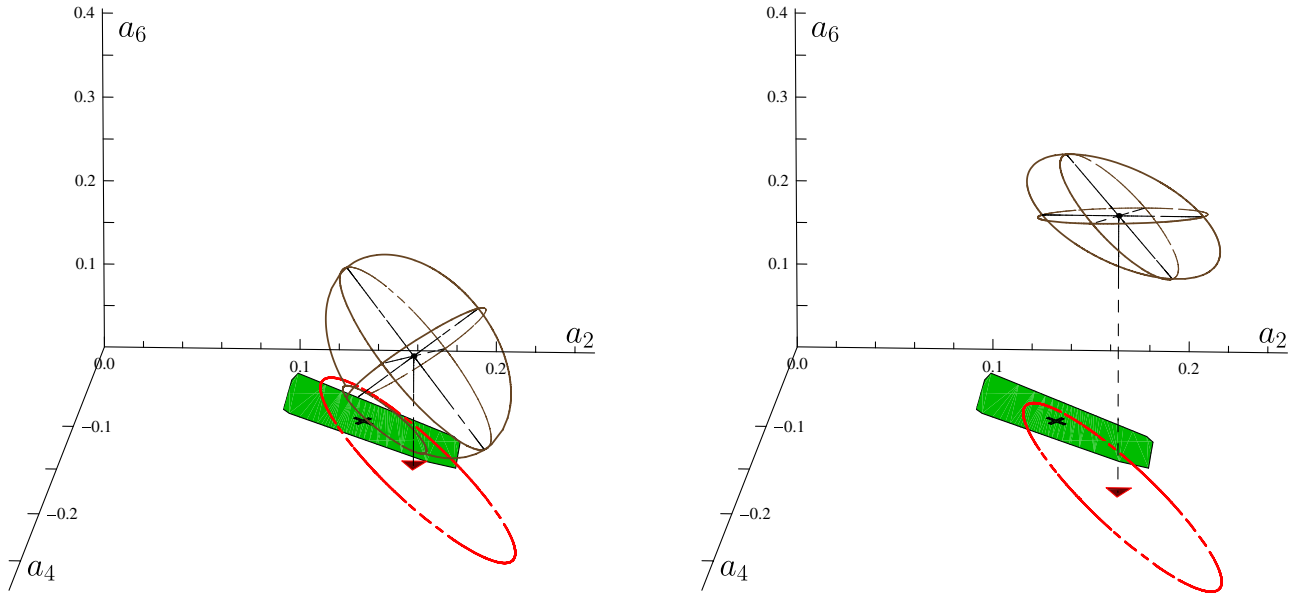

FIG. 2 (color online). 3D graphics of 1σ error ellipsoids in the space spanned by the Gegenbauer coefficients a_n $(n = 2, 4, 6)$ of all data [5–7] on the pion-photon transition form factor in the range $[1 \div 9]$ GeV^2 (left panel) and $[1 \div 40]$ GeV^2 (right panel) processed with the help of LCSRs (details in the text). The projection of the 1σ ellipsoid on the plane (a_2, a_4) is represented, in both panels, by the larger ellipse in red color. The smaller ellipse denotes the cross section of the ellipsoid with the (a_2, a_4) plane. The shaded (green) rectangle encloses the region of those a_2, a_4 pairs that are allowed by NLC SRs [17], whereas its middle point (×) marks the BMS pion DA. All results are shown at the scale $\mu^2_{\rm SY}$ after NLO evolution.

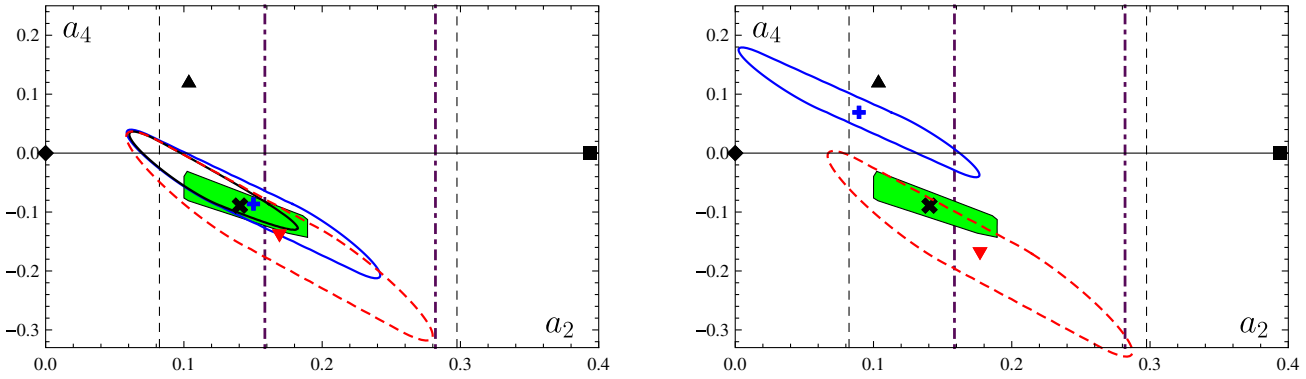

FIG. 3 (color online). Distorted 1σ error ellipses of the $F^{\gamma^*\gamma\pi}(Q^2)$ data in the range $[1 \div 9]$ GeV^2 (left panel) and $[1 \div 40]$ GeV^2 (right panel) from various experiments [5–7,25] using different data-analysis procedures. These ellipses (see text for explanations) are the result of unifying different ellipses which correspond to the twist-four parameter varying in the range $\delta^2 = 0.15 \div 0.23$ GeV^2. The slanted rectangle in green color encloses the area of a_2 and a_4 values determined by NLC SRs [17], with the BMS pion DA being marked by $\times$. The middle points of the ellipses are also labeled [+ and ▼ (red)] together with the asymptotic DA (◆), the CZ DA (■), and Model III from [9] (▲). The vertical lines indicate the range of a_2 values determined by two lattice simulations: [39]—dashed lines; [40]—dashed-dotted (blue) lines. The Borel parameter $M^2(Q^2)$ is varied with Q^2 in both panels as explained in the text. All results are shown at the scale $\mu^2_{\rm SY}$.

all *BABAR* data up to the highest measured value of Q^2. To this end, we calculate the 1σ error ellipses by allowing the parameter δ^2 to vary by 20% around the value 0.19 GeV^2. All ellipses obtained this way are then merged together into a single distorted 1σ error ellipse shown in Fig. 3 for different situations. These are the following: The largest ellipse—dashed line in red color with the middle point ▼—represents the result of combining the projections on the plane (a_2, a_4) of the 3D data analysis. The smaller ellipse (solid blue line) shows the analogous result of a 2D analysis by means of a_2 and a_4. Its middle point + with the coordinates $(0.15, -0.09)$ and $\chi^2_{\rm ndf} \approx 0.5$, almost coincides with the middle point $\times$ of the area of values determined by NLC SRs. Finally, the smallest ellipse (thick line), entirely enclosed by the previous one, is obtained by combining the intersections with the (a_2, a_4) plane of all ellipsoids generated by the variation around the central value of δ^2. The ellipsoid that corresponds to the central value $\delta^2 = 0.19$ GeV^2 is shown in the left panel of Fig. 2.

The locations in the (a_2, a_4) plane of some characteristic pion DAs are also indicated in Fig. 3; notably, the asymptotic DA (◆), the CZ model (■), and also the projection of Model III from [9] (▲). It is worth emphasizing that the slanted (green) rectangle that contains those values of a_2 and a_4 derived from NLC SRs [17] lies almost completely within both larger error ellipses—greatly overlapping with the smallest one as well. In particular, the BMS model DA $\times$ turns out to be inside of all 1σ error ellipses. Hence, the results of the 2D and 3D data analyses are in good mutual agreement, while we observe no tension between them and the theoretical predictions obtained from NLC SRs [17]—at least at the level of $\chi^2_{\rm ndf} \leq 0.5$. What is more, all calculated 1σ error ellipses are complying fairly well with the boundaries for a_2 provided by two independent lattice simulations. The older estimate from [39] is indicated in both panels of this figure by the vertical dashed lines, whereas the very recent results given in Ref. [40] (Table XII there) are denoted by the dashed-dotted vertical lines in blue color.

As one can see from the right panel of Fig. 3, the situation changes considerably when the high-Q^2 tail of the *BABAR* data [7] is included in the data analysis. Using the same designations as in the left panel, we show the analogous unified error ellipses, observing that now the ellipsoid has no intersection with the (a_2, a_4) plane. Moreover, the composed error ellipse resulting from the 2D analysis (solid blue line) moves out of the region of the negative values of a_4 and inside its positive domain. This is accompanied by the significantly worse value $\chi^2_{\rm ndf} \approx 2$, in sharp contrast to the value $\chi^2_{\rm ndf} \approx 0.5$ we found for the data set in the CLEO regime. On the other hand, the unified 1σ error ellipse of the 3D projections on the (a_2, a_4) plane (larger dashed red ellipse), keeps its position unchanged and still harbors a big portion of the area for the a_2, a_4 values, compatible with the results from NLC SRs (shaded rectangle in green color).

Comparison with the lattice findings shows that the 3D error ellipse lies almost entirely within the boundaries from [39] (dashed vertical lines) but intersects with the interval determined in [40] (dashed-dotted vertical lines) only for the larger values of a_2. The analogous ellipse of the 2D analysis only poorly complies with this small a_2 window of [40], whereas it partly overlaps with the low end of the a_2 range determined in [39]. Thus, the mutual agreement between the 2D and the 3D analysis, observed in the left panel, now deteriorates. Moreover, it becomes obvious from this figure that Model III from [9] has a projection

on the (a_2, a_4) plane that lies outside of all considered 1σ error ellipses of the data. Note incidentally that selecting for the Borel parameter the value $M^2 = 1.5$ GeV^2, as used in [9], we find for their Model III an agreement with the *BABAR* data on the level of $\chi^2_{\rm ndf} \gtrsim 1.5$.

This discussion becomes more substantiated by inspecting Fig. 4 which compares theoretical predictions with various experimental data with appropriate designations provided in the figure. Our calculations are displayed in the form of a shaded strip (green color) with a width reflecting various theoretical uncertainties. These are (i) uncertainties owing to the spread of the bunch of the pion DAs derived in [17], (ii) those originating from the variation of the twist-four parameter δ^2, and (iii) those related to the sum of the NNLO β_0 term and the twist-six contribution [9]. Because these two latter contributions are comparable in size, they almost mutually cancel. For a more detailed understanding, we have compiled the calculated form-factor values for the BMS DA at each measured point in Table I (last column), including also the aforementioned theoretical errors. Note that the first error originates from items (i) and (ii), whereas the second one stems from item (iii).

As one clearly sees from Fig. 4, these predictions (shaded strip in green color), obtained with LCSRs within the standard collinear factorization scheme of QCD, cannot reproduce the significant rise of the high-Q^2 tail of the $\gamma^*\gamma \to \pi^0$ *BABAR* data [7]. But, surprisingly, they are in very good agreement with the *BABAR* data for the

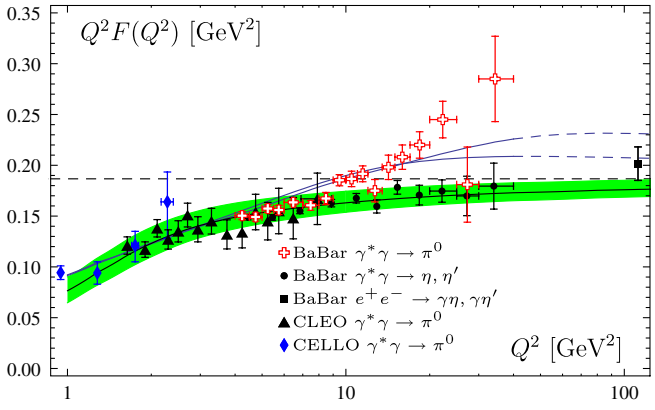

FIG. 4 (color online). Predictions for the scaled form factor $Q^2F^{\gamma^*\gamma\pi}(Q^2)$ using a logarithmic scale for Q^2. The predictions using the BMS bunch of π DAs are displayed in the form of a shaded (green) strip, with the solid line denoting the BMS model [17]. The width of the strip contains various theoretical uncertainties explained in the text. The two single solid (blue) lines reproduce the predictions of Agaev *et al.* [9] with their models I and III, whereas the prediction using their model II—not shown—would be in between. (For the sake of comparison, we extended these predictions beyond 40 GeV^2 in the form of dashed lines up to the remote point of 112 GeV^2). The experimental data are taken from various experiments [5–7,25,41].

two-photon η and η' decays [25] using the description of the η-η' mixing in the quark flavor basis [42]. These data are also shown in the fifth column of Table I. Under the assumption that the state $|n\rangle = (|\bar{u}u\rangle + |\bar{d}d\rangle)/\sqrt{2}$ has a DA similar to that of the pion, one can link the $\gamma^*\gamma \to |n\rangle$ transition form factor, multiplied by $3/5$, to the form factor $\gamma^*\gamma \to \pi^0$, where the prefactor arises from the quark charges. Strictly speaking, one should compare the state π^0 not with the physical particles η and η' but with the other neutral states η_1 and η_8 of the pseudoscalar meson sector. The observed discrepancy of the two *BABAR* data sets indicates that the structure of η_8 is very different from that of π^0, which looks implausible in view of the fact that both these states belong to the octet (a detailed discussion of this issue is given in [33,34]). Whether this is a true dynamical effect or accidental cannot be answered rigorously at present. One realizes from this figure that two *BABAR* data points for the $\gamma^*\gamma \to \pi^0$ measurement [7] at $Q^2 = 12.7$ GeV^2 and 27.3 GeV^2 also lie inside the shaded strip, being perfectly in line with the data for the $|n\rangle$ form factor. Moreover, our predictions (shaded strip) approach, together with these data, the asymptotic QCD limit $\sqrt{2}f_\pi$ from below. In marked contrast, the predictions derived by Agaev *et al.* [9]—single solid lines in this figure—fail to comply with these data and exceed considerably the asymptotic QCD limit. Unfortunately, they even fail to provide agreement with the $\gamma^*\gamma \to \pi^0$ *BABAR* data as well. Indeed, as one sees from Fig. 4, the characteristic rise of these data with Q^2 beyond 10 GeV^2 cannot be reproduced, mainly because the enhancement provided by a large and positive coefficient a_4 is not really sufficient—even augmenting it with the inclusion of some more higher coefficients $a_6, \ldots$—so that the form factor gradually flattens out instead of increasing with Q^2. However, in view of the fluctuations of the *BABAR* data at higher Q^2 values, one cannot rule out a flatter behavior than the fit in Eq. (8) proposed by *BABAR*. To quantify the above statements and facilitate comparisons with other approaches, we collect in Table II the statistical properties pertaining to the data fits, using various sets of data and selected pion DA models. Let us also mention that the variation of the lower bound of Q^2 in the statistical analysis, e.g., the exclusion of the lowest six experimental points to prevent a strong influence of twist-four uncertainty, does not affect the pattern of the $\chi^2_{\rm ndf}$ values of the BMS DA, Asy DA, and the CZ DA, shown in Table II. A detailed analysis of the variation of the lower bound in Q^2 has been given in [16].

Be that as it may, the most immediate conclusion is that the *BABAR* data for the pion and the $|n\rangle$ state seem antithetical and cannot be equally reproduced within the standard QCD scheme.

The accuracy of the experimental data on $\gamma^*\gamma \to \pi^0$ and the precision of current lattice simulations in extracting constraints on the second moment $\langle \xi^2 \rangle_\pi$ of the pion DA

TABLE I. Results for the scaled pion-photon transition form factor calculated in this work (last column) in comparison with the values measured at the same momentum scales by the CLEO [6] and the *BABAR* [7,25] collaborations, both for the $\gamma^*\gamma \to \pi^0$ and the $\gamma^*\gamma \to |n\rangle$ decays. The last entry at the timelike momentum $\tilde{Q}^2 = 112$ GeV^2 is taken from [41]. The origin of the theoretical uncertainties in the last column is explained in the text.

CLEO/*BABAR*	CLEO/*BABAR*	CLEO	*BABAR*	*BABAR* (η, η')	This work
Q^2 interval [GeV^2]	$\tilde{Q}^2$ [GeV^2]	$\tilde{Q}^2\lvert F^{\gamma^*\gamma\pi^0}_{\rm CLEO}(\tilde{Q}^2)\rvert$ [0.01 × GeV]	$\tilde{Q}^2\lvert F^{\gamma^*\gamma\pi^0}_{BaBar}(\tilde{Q}^2)\rvert$ [0.01 × GeV]	$(3/5)\tilde{Q}^2\lvert F^{\gamma^*\gamma n}_{BaBar}(\tilde{Q}^2)\rvert$ [0.01 × GeV]	$\tilde{Q}^2\lvert F^{\gamma^*\gamma\pi^0}(\tilde{Q}^2)\rvert$ [0.01 × GeV]
1.5–1.8	1.64	$12.1 \pm 0.8 \pm 0.3$	...	...	$11.14^{+1.06+0.5}_{-1.02-0.3}$
1.8–2.0	1.90	$11.7 \pm 0.7 \pm 0.3$	...	...	$12.04^{+1.09+0.5}_{-1.03-0.3}$
2.0–2.2	2.10	$13.8 \pm 0.8 \pm 0.3$	...	...	$12.58^{+1.09+0.5}_{-1.01-0.3}$
2.2–2.4	2.30	$12.7 \pm 0.9 \pm 0.3$	...	...	$13.03^{+1.07+0.5}_{-0.99-0.3}$
2.4–2.6	2.50	$13.5 \pm 1.0 \pm 0.3$	...	...	$13.4^{+1.04+0.5}_{-0.95-0.3}$
2.6–2.8	2.70	$15.1 \pm 1.1 \pm 0.4$	...	...	$13.71^{+1.01+0.5}_{-0.92-0.3}$
2.8–3.1	2.94	$13.7 \pm 1.2 \pm 0.3$	...	...	$14.02^{+0.99+0.5}_{-0.90-0.3}$
3.1–3.5	3.29	$14.5 \pm 1.2 \pm 0.4$	...	...	$14.38^{+0.96+0.5}_{-0.88-0.3}$
3.5–4.0	3.74	$13.2 \pm 1.4 \pm 0.3$	...	...	$14.73^{+0.92+0.5}_{-0.85-0.3}$
4.0–4.5	4.24	$13.4 \pm 1.5 \pm 0.3$	15.04 ± 0.39	...	$15.02^{+0.87+0.5}_{-0.82-0.3}$
4.0–5.0	4.44	...	...	14.89 ± 0.26	$15.12^{+0.86+0.5}_{-0.80-0.3}$
4.5–5.0	4.74	$15.4 \pm 1.7 \pm 0.4$	14.91 ± 0.41	...	$15.25^{+0.83+0.5}_{-0.79-0.3}$
5.0–5.5	5.24	$14.5 \pm 1.8 \pm 0.4$	15.74 ± 0.39	...	$15.43^{+0.80+0.5}_{-0.76-0.3}$
5.0–6.0	5.45	...	...	14.86 ± 0.27	$15.49^{+0.79+0.5}_{-0.75-0.3}$
5.5–6.0	5.74	$15.5 \pm 2.2 \pm 0.4$	15.60 ± 0.45	...	$15.58^{+0.77+0.5}_{-0.74-0.3}$
6.0–7.0	6.47	$14.8 \pm 2.0 \pm 0.4$	16.35 ± 0.36	...	$15.76^{+0.74+0.5}_{-0.71-0.3}$
6.0–8.0	6.85	...	...	15.52 ± 0.28	$15.84^{+0.73+0.5}_{-0.70-0.3}$
7.0–8.0	7.47	...	16.06 ± 0.47	...	$15.96^{+0.71+0.5}_{-0.68-0.3}$
7.0–9.0	7.90	$16.7 \pm 2.5 \pm 0.4$	...	...	$16.03^{+0.69+0.5}_{-0.67-0.3}$
8.0–9.0	8.48	...	16.73 ± 0.60	...	$16.12^{+0.68+0.5}_{-0.65-0.3}$
8.0–10.0	8.87	...	...	16.27 ± 0.37	$16.17^{+0.67+0.5}_{-0.65-0.3}$
9.0–10.0	9.48	...	18.53 ± 0.55	...	$16.25^{+0.65+0.5}_{-0.64-0.3}$
10.0–11.0	10.48	...	18.66 ± 0.76	...	$16.36^{+0.63+0.5}_{-0.62-0.3}$
10.0–12.0	10.90	...	...	16.76 ± 0.47	$16.4^{+0.63+0.5}_{-0.61-0.3}$
11.0–12.0	11.49	...	19.16 ± 0.78	...	$16.45^{+0.62+0.5}_{-0.61-0.3}$
12.0–13.5	12.71	...	17.5 ± 1.1	...	$16.55^{+0.60+0.5}_{-0.59-0.3}$
12.0–14.0	12.91	...	...	15.95 ± 0.65	$16.57^{+0.60+0.5}_{-0.59-0.3}$
13.5–15.0	14.22	...	19.8 ± 1.2	...	$16.65^{+0.58+0.5}_{-0.58-0.3}$
14.0–17.0	15.31	...	...	17.83 ± 0.67	$16.72^{+0.57+0.5}_{-0.57-0.3}$
15.0–17.0	15.95	...	20.8 ± 1.2	...	$16.75^{+0.57+0.5}_{-0.56-0.3}$
17.0–20.0	18.40	...	22.0 ± 1.3	17.06 ± 0.97	$16.86^{+0.55+0.5}_{-0.55-0.3}$
20.0–25.0	22.28	...	24.5 ± 1.8	17.46 ± 1.10	$16.99^{+0.53+0.5}_{-0.53-0.3}$
25.0–30.0	27.31	...	$18.1 - 4.0 + 3.3$	16.98 ± 1.94	$17.11^{+0.51+0.5}_{-0.51-0.3}$
30.0–40.0	34.36	...	$28.5 - 4.5 + 3.9$	17.95 ± 2.26	$17.23^{+0.49+0.5}_{-0.49-0.3}$
-	112	...	...	20.16 ± 1.65	$17.63^{+0.42+0.5}_{-0.43-0.3}$

have both reached a level that can be used to determine the range of values of the next moment $\langle\xi^4\rangle_\pi$, where both experimental data and lattice computations overlap. This possibility was first pointed out in [43] and the following range of values was extracted from the 1σ error ellipse of the CLEO data [6] in conjunction with the lattice constraints for $\langle\xi^2\rangle_\pi$ from [44]: $\langle\xi^4\rangle_\pi \in [0.095 \div 0.134]$ at $\mu^2_{\rm Lat} = 4$ GeV^2 and for $M^2 = 0.7$ GeV^2. Here we refine this procedure in the following way: first, we map the (a_2, a_4) plane onto the $(\langle\xi^2\rangle_\pi, \langle\xi^4\rangle_\pi)$ plane. Then, we combine the mapped 1σ error ellipse (area enclosed by a solid blue line) in Fig. 5 for the data sets in the CLEO regime (cf. Fig. 3) with the constraints from [39] and [40] (Table XII there), the aim being to extract that range of values of $\langle\xi^4\rangle_\pi$ where they overlap. The corresponding results at the typical lattice scale

TABLE II. Statistical properties of selected pion DA models (first column) with corresponding coefficients a_n (second column) used in the calculation of the pion-photon transition form factor by means of LCSRs. The last two columns show the values of $\chi^2_{\rm ndf} \equiv \chi^2/{\rm ndf}$ for the data in the CLEO regime and for the whole set of the data, respectively.

π DA model	$(a_2, a_4, \ldots)\mu^2 = \mu^2_{\rm SY}$	$\chi^2_{\rm ndf}$ (1–9 GeV^2)	$\chi^2_{\rm ndf}$ (1–40 GeV^2)
BMS DA ($\times$)	(0.141, −0.089)	0.5	3.1
Asy DA (◆)	(0,0)	4.7	7.9
CZ DA (■	(0.394,0)	32.3	25.5
Model I [9]	(0.084,0.137,0.088,0.063,0.048,0.039)	2.8	2.4
Model III [9] (▲)	(0.104,0.123,0.039)	3.2	2.8

$\mu^2_{\rm Lat} = 4\,{\rm GeV}^2$ are, respectively, (i) $\langle\xi^2\rangle_\pi \in [0.23 \div 0.29]$ and $\langle\xi^4\rangle_\pi \in [0.102 \div 0.122]$, (ii) $\langle\xi^2\rangle_\pi \in [0.26 \div 0.29]$ and $\langle\xi^4\rangle_\pi \in [0.11 \div 0.122]$. These windows were extracted by employing a Q^2-dependent Borel parameter, as before in this analysis. Using instead $M^2 = 1.5$ GeV^2, as in [9], one would obtain only a small intersection of the corresponding region, shown in Fig. 5 by the dashed (red) line, with the lattice constraints of [39], amounting to the value $\langle\xi^4\rangle_\pi \simeq 0.1$, while there would be no intersection at all with the lattice estimates of [40]. The sensitivity of $\langle\xi^2\rangle_\pi$ on the choice of the Borel parameter M^2 provides a handle to consider the existing lattice computations [39,40] as providing independent evidence in support of the original prescription for the Borel parameter in the LCSRs for the pion-photon transition form factor [8,11].

V. SUMMARY AND CONCLUSIONS

In summary, three different sets of experimental data on the pion-photon transition form factor have been analyzed with the help of QCD LCSRs along the lines of our earlier works in [15,16] and adopting the reasoning expressed in [8,11]. The following key ingredients have been taken into account: (i) the NLO radiative correction, (ii) the twist-four contribution, and (iii) the NNLOβ_0 QCD correction [23,24] together with the recently computed [9] twist-six contribution, these two by means of theoretical uncertainties. This is possible in our approach because in the range of the Borel parameter adopted, $M^2 < 1.0$ GeV^2, these two corrections, though with opposite signs, have almost the same absolute (not large) magnitude. Carrying out the analysis, evidence has been obtained that the data from CELLO [5], CLEO [6], and *BABAR* [7] between 1 and 9 GeV^2 favor a pion distribution amplitude with endpoint suppression, like the BMS model [17] (see the left panels of Figs. 2 and 3). The key for the overlap between the error ellipses of the data in the (a_2, a_4) plane with the allowed region from NLC SRs is a *negative* value of the Gegenbauer coefficient $|a_4| \lesssim a_2$. Beyond 10 GeV^2, the best fit to the *BABAR* data on $F^{\gamma^*\gamma\to\pi^0}(Q^2)$ requires a sizeable coefficient a_6 comparable with the lower coefficients (cf. right panel of Fig. 2).

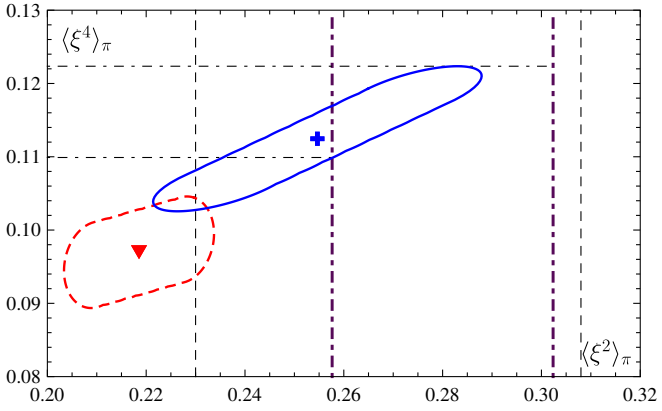

FIG. 5 (color online). Predictions for the moments $\langle\xi^2\rangle_\pi$ and $\langle\xi^4\rangle_\pi$ at the lattice scale $\mu^2_{\rm Lat} = 4$ GeV^2. The solid (blue) ellipse corresponds to our choice of M^2, whereas the dashed (red) one results when using $M^2 = 1.5$ GeV^2. The vertical lines show the range of values computed on the lattice: dashed line—[39]; dashed-dotted (violet) line—[40].

The comparison of our theoretical predictions for the scaled form factor $Q^2F^{\gamma^*\gamma\pi}(Q^2)$ in Fig. 4 makes it apparent that there is an antithetic trend between the *BABAR* data on the pion-gamma transition form factor [7] and those extracted from the $\gamma^*\gamma \to \eta(\eta')$ transition form factors [25]. While the latter agree very well with the BMS predictions (solid line in Fig. 1 and shaded strip in Fig. 4), the high-Q^2 tail of the π^0 *BABAR* data requires a pion DA with sizeable (or even growing with n) higher Gegenbauer coefficients a_n, or alternative theoretical schemes outside the standard QCD factorization approach, see, e.g., [26,27,30,45,46]. Similar conclusions were also drawn in [47] using Dyson–Schwinger equations.

This intriguing behavior of the *BABAR* data cannot be reconciled with QCD factorization in combination with LCSRs, despite the opposite claims expressed in [9]. As one sees from Fig. 4, this is not possible for our choice of the Borel window $M^2 \approx 0.7 - 0.9$ GeV^2, giving rise to the shaded strip, but also not for the higher values $M^2 = 1.5 \pm 0.5$ GeV^2 employed in [9] (single solid lines in the same figure). Even a large positive coefficient a_4 and a sizeable value of a_6 cannot provide sufficient reinforcement of the

$\gamma^*\gamma \to \pi^0$ form factor to bridge the gap to the high-Q^2 *BABAR* data and reproduce their increase with Q^2 without the loss of the statistical accuracy. Quantitatively, this means that involving in the 3D data analysis the high-Q^2 tail of the *BABAR* data, makes the description inevitably worse ($\chi^2_{\rm ndf} \geq 1$) in comparison with the analysis applicable to the CLEO regime ($\chi^2_{\rm ndf} \approx 0.4$). Remarkably, also the recent light-front holographic analysis in Ref. [34] yields predictions which are incompatible with the strong rise of the *BABAR* data at high Q^2, while being in agreement with those extracted from the $\gamma^*\gamma \to \eta(\eta')$ transition form factors and rather close to our results in this region.

The bottom line is, new measurements, e.g., by the Belle Collaboration, may help resolve the controversies around the *BABAR* data and understand the dichotomy between the pion and the state $|n\rangle$ that indicates a strong violation of flavor symmetry. In addition, a precise lattice estimate of $\langle\xi^4\rangle_\pi$ could be instrumental in fixing the sign of the Gegenbauer coefficient a_4 of the pion DA. Moreover, our detailed predictions in Table I in conjunction with Fig. 4 may serve as a sort of "reference model" for various purposes—theoretical and experimental.

ACKNOWLEDGMENTS

We would like to thank Anatoly Efremov, Simon Eidelman, Andrei Kataev, and Dmitri Naumov for stimulating discussions and useful remarks. A. B., S. M., and A. P. are thankful to Professor Evgeny Epelbaum and Professor Maxim Polyakov for the warm hospitality at Bochum University, where the major part of this investigation was carried out. A. B., S. M., and A. P. acknowledge financial support from Nikolay Rybakov. A. P. also wishes to thank the Ministry of Education and Science of the Russian Federation ("Development of Scientific Potential in Higher Schools" projects No. 2.2.1.1/12360 and No. 2.1.1/10683). This work was supported in part by the Heisenberg–Landau Program under Grant 2011, the DAAD (A. P.), the Russian Foundation for Fundamental Research (Grant No. 09-02-01149), and the BRFBR JINR Cooperation Program under Contract No. F10D-002.

[1] S. J. Brodsky and G. P. Lepage, Adv. Ser. Dir. High Energy Phys. **5**, 93 (1989).
[2] A. V. Efremov and A. V. Radyushkin, Phys. Lett. B **94**, 245 (1980); Theor. Math. Phys. **42**, 97 (1980).
[3] G. P. Lepage and S. J. Brodsky, Phys. Rev. D **22**, 2157 (1980).
[4] A. V. Radyushkin, arXiv:hep-ph/0410276.
[5] H. J. Behrend *et al.*, Z. Phys. C **49**, 401 (1991).
[6] J. Gronberg *et al.*, Phys. Rev. D **57**, 33 (1998).
[7] B. Aubert *et al.*, Phys. Rev. D **80**, 052002 (2009).
[8] A. Khodjamirian, Eur. Phys. J. C **6**, 477 (1999).
[9] S. S. Agaev, V. M. Braun, N. Offen, and F. A. Porkert, Phys. Rev. D **83**, 054020 (2011).
[10] K. Nakamura *et al.*, J. Phys. G **37**, 075021 (2010).
[11] A. Schmedding and O. Yakovlev, Phys. Rev. D **62**, 116002 (2000).
[12] V. M. Braun and I. E. Filyanov, Z. Phys. C **44**, 157 (1989).
[13] A. P. Bakulev, S. V. Mikhailov, and N. G. Stefanis, Phys. Rev. D **73**, 056002 (2006).
[14] V. L. Chernyak and A. R. Zhitnitsky, Phys. Rep. **112**, 173 (1984).
[15] A. P. Bakulev, S. V. Mikhailov, and N. G. Stefanis, Phys. Rev. D **67**, 074012 (2003).
[16] A. P. Bakulev, S. V. Mikhailov, and N. G. Stefanis, Phys. Lett. B **578**, 91 (2004).
[17] A. P. Bakulev, S. V. Mikhailov, and N. G. Stefanis, Phys. Lett. B **508**, 279 (2001); **590**, 309(E) (2004).
[18] A. P. Bakulev and A. V. Pimikov, Acta Phys. Pol. B **37**, 3627 (2006); Phys. Part. Nucl. **4**, 377 (2007).
[19] A. P. Bakulev, in *New Trends in High-Energy Physics, Yalta (Crimea), 16–23 Sept., 2006*, edited by P. N. Bogolyubov *et al.* (BITP NASU (Kiev), JINR (Dubna), Kiev, 2006), pp. 203–212.
[20] A. P. Bakulev, S. V. Mikhailov, and N. G. Stefanis, Ann. Phys. (Leipzig) **13**, 629 (2004).
[21] V. M. Braun, E. Gardi, and S. Gottwald, Nucl. Phys. **B685**, 171 (2004).
[22] S. S. Agaev, Phys. Rev. D **72**, 114010 (2005); **73**, 059902 (E) (2006).
[23] S. V. Mikhailov and N. G. Stefanis, Nucl. Phys. **B821**, 291 (2009).
[24] B. Melić, D. Müller, and K. Passek-Kumerički, Phys. Rev. D **68**, 014013 (2003).
[25] P. d. A. Sanchez *et al.*,, arXiv:1101.1142.
[26] A. V. Radyushkin, Phys. Rev. D **80**, 094009 (2009).
[27] M. V. Polyakov, JETP Lett. **90**, 228 (2009).
[28] S. V. Mikhailov, A. V. Pimikov, and N. G. Stefanis, Phys. Rev. D **82**, 054020 (2010).
[29] V. L. Chernyak, arXiv:0912.0623.
[30] A. E. Dorokhov, Phys. Part. Nucl. **7**, 229 (2010).
[31] H.-n. Li and S. Mishima, Phys. Rev. D **80**, 074024 (2009).
[32] X.-G. Wu and T. Huang, Phys. Rev. D **82**, 034024 (2010).
[33] P. Kroll, Eur. Phys. J. C **71**, 1623 (2011).
[34] S. J. Brodsky, F.-G. Cao, and G. F. de Teramond, Phys. Rev. D **84**, 033001 (2011); arXiv:1105.3999.
[35] P. Kroll and M. Raulfs, Phys. Lett. B **387**, 848 (1996).
[36] N. G. Stefanis, W. Schroers, and H.-C. Kim, Phys. Lett. B **449**, 299 (1999); Eur. Phys. J. C **18**, 137 (2000).
[37] A. I. Karanikas and N. G. Stefanis, Phys. Lett. B **504**, 225 (2001); **636**, 330(E) (2006).

[38] M. A. Shifman, A. I. Vainshtein, and V. I. Zakharov, Nucl. Phys. **B147**, 385 (1979).
[39] V. M. Braun *et al.*, Phys. Rev. D **74**, 074501 (2006).
[40] R. Arthur *et al.*, Phys. Rev. D **83**, 074505 (2011).
[41] B. Aubert *et al.*, Phys. Rev. D **74**, 012002 (2006).
[42] T. Feldmann, P. Kroll, and B. Stech, Phys. Rev. D **58**, 114006 (1998).
[43] N. G. Stefanis, Nucl. Phys. B, Proc. Suppl. **181–182**, 199 (2008).
[44] M. A. Donnellan *et al.*, Proc. Sci., LAT2007 (2007) 369.
[45] Y. N. Klopot, A. G. Oganesian, and O. V. Teryaev, Phys. Lett. B **695**, 130 (2011).
[46] A. Stoffers and I. Zahed, arXiv:1104.2081.
[47] H. L. L. Roberts, C. D. Roberts, A. Bashir, L. X. Gutierrez-Guerrero, and P. C. Tandy, Phys. Rev. C **82**, 065202 (2010).